RSC Advances

PAPER

View Article Online
View Journal | View Issue

Cite this: *RSC Adv.*, 2023, **13**, 33255

Fluorescent dual-mode sensor for the determination of graphene oxide and catechin in environmental or food field†

Esther Pinilla-Peñalver, [ab] Adrián Esteban-Arranz, [cd] Ana M. Contento [a] and Ángel Ríos *[a]

The novel fluorescent sensor is proposed in this work based on the competitive interactions between the known bioactive compounds, riboflavin and catechin, which act as guests, and graphene oxide (GO) material that acts as host. Specifically, this proposal is based on an indicator displacement assay which allows the detection of GO and catechin (fluorescence quenching of riboflavin signal by GO and increase in fluorescence by catechin on the GO–riboflavin system). Three GO structures with different lateral dimensions and thickness were synthesized and tested, being able to be the three differentiated depending on the attenuation capacity of the fluorescent signal that each one possesses. The environmental analytical control of GO is more and more important, being this method sensitive and selective in the presence of other potential interferent substances. On the other hand, the other sensing capacity of the sensor also allows the determination of catechin in food samples based on the formation of riboflavin–GO complex. It is a rapid, simple and non-expensive procedure. Thus, the same 2D nanomaterial (GO) is seen to play a double role in this sensing strategy (analyte and analytical tool for the determination of another compound).

Received 14th July 2023
Accepted 22nd October 2023

DOI: 10.1039/d3ra04726a

rsc.li/rsc-advances

Introduction

Graphene-based nanomaterials are two-dimensional layers composed of large sp^2 hybridized carbon atoms in a hexagonal configuration. In this broad family graphene oxide (GO) is considered as a heterogeneous structure that is rich in oxygen functional groups such as hydroxyl and epoxy at the basal plane and carboxylic groups at the edges.[1] Unlike graphene, the presence of functional groups in the material involves the existence of sp^3 carbon atoms that widen the optical bandgap, giving rise to fluorescent materials.[2] GO is typically prepared by the oxidation of graphite with strong acids and other oxidants followed by an exfoliation step. Analogous graphene and reduced graphene oxide (rGO) present lesser or no functionalization (compared to GO) and are, therefore, less stable than GO in aqueous media.[3] One of the most advantages of carbon-based materials is their large specific surface area in comparison to many other nanoparticle.[4] This physical characteristic makes them suitable for the adsorption of organic molecules *via* non-covalent interactions, π–π interactions, electrostatic forces, van der Waals, hydrogen bonding or hydrophobic interactions.[5] It is due to their unique properties that graphene-based nanomaterials are increasingly applied in the environment, biomedicine and food safety. Thus, in recent years, GO has been applied in fluorescent sensors not only as a fluorophore but also as an effective fluorescence quencher,[2,6,7] through either non-fluorescent complex formation, charge transfer or Förster resonance energy transfer (FRET) processes. The limitation to employ GO as a fluorescent label lies in its broad emission peak, which limits the detection performance when the spectral intensity of fluorescence is transduced as a signal.[2] However, few fluorescence sensors related to the competitive adsorption of chemical compounds on GO-based materials surface have previously been reported.[1,8,9]

Intensive production of nanomaterials at industrial scale, as well as their commercialization in consumer products, such as electronic devices, cosmetics, food and drugs will increase the human and environmental exposure to these nanomaterials. Their release into the environment could presents several risks to human health and ecosystem,[3,10] so, it is necessary to evaluate their possible effects. Specifically, GO nanostructures could reach the environment through atmospheric emissions, transport pollution and waste from production and research facilities, contaminating the soil, surface and groundwater, even

[a]*Department of Analytical Chemistry and Food Technology, University of Castilla-La Mancha, Avenue Camilo José Cela, s/n, 13071 Ciudad Real, Spain. E-mail: Angel.Rios@uclm.es; Esther.Pinilla@uclm.es; AnaMaria.Contento@uclm.es; Tel: +34926295232*

[b]*Regional Institute for Applied Chemistry Research, IRICA, Avenue Camilo José Cela, 1, 13071 Ciudad Real, Spain*

[c]*Department of Chemical Engineering, University of Castilla La-Mancha, Avenue Camilo José Cela, 12, 13071, Ciudad Real, Spain. E-mail: adrian.esteban@ictp.csic.es*

[d]*Department of Polymeric Nanomaterials and Biomaterials, Polymer Science and Technology Institute (CSIC), Juan de la Cierva 3, 28006, Madrid, Spain*

† Electronic supplementary information (ESI) available. See DOI: https://doi.org/10.1039/d3ra04726a

affecting the organisms present there.[11] Therefore, analytical methods are increasingly needed for the characterization and determination of engineered nanomaterials in complex matrices.[12] Despite this, some approaches have been developed for the quantification of metallic nanoparticles,[13,14] carbon-based nanomaterials[15,16] and nanostructured organic materials.[17,18] However, to the best of our knowledge, GO-based sensors found in the literature in which GO is used as a quencher do not quantitatively determine the nanomaterial.

Furthermore, catechin belongs to the representative family of flavonoids, specifically flavan-3-ols, and involves four diastereoisomers, being the most common isomer of catechin the (+)-catechin. Favan-3-ol compounds present diverse beneficial effects related to human health based on antioxidative, anti-inflammatory, anti-microbial, anti-cancer, cardioprotective and neuroprotective properties, among many others.[19,20] All the properties of catechin arises from its polyphenolic structure, which enables to exhibit a strong antioxidant activity. Some of the natural sources where catechins are commonly found are fresh tea leaves, red wine, cocoa beans, grapes and raspberries.[21] As a biologically active compound, this type of flavanol contributes in many of the characteristics that make these natural products essential for the human diet. The content of catechins is an important parameter for the evaluation of many food products quality such as tea or cocoa.[22] To date, the determination of catechin content in food samples was mostly carried out based on high-performance liquid chromatography-UV/fluorescent detection (HPLC-UV/FL), gas chromatography-mass spectrometry (GC-MS) and capillary electrophoresis-UV (CE-UV).[23–27] However, HPLC-DAD/FL, GC-MS or CE-DAD require complex separation and determination systems and long analysis times. Compared to the above methods, fluorescence technology is highly efficient and easy to operate and it has become an effective method for routine analysis.[22]

For both reasons mentioned above, a novel turn-off-on fluorescence approach based on the affinity of a fluorescent essential vitamin (B_2), riboflavin, for GO surface in comparison to catechin was developed. GO showed to act both as an effective nanoquencher and as a highly selective nanoadsorbent. This fact allowed its quantification, being of great relevance since at present the development of techniques and methodologies for the determination and quantification of nanomaterials is still necessary. Moreover, this study demonstrates the competitive interactions between GO and riboflavin or catechin allowing the flavonoid detection. The applicability of this strategy for both GO and catechin determination in environmental and food matrices was successfully carried out.

Materials and methods

Information related to reagents and materials and instruments is given in the ESM.S1†

Analytical procedure for the analysis of GO and catechin

Working solutions of large graphene oxide (lGO, 0.42 mg mL^{-1}), small graphene oxide (sGO, 0.47 mg mL^{-1}) and monolayer graphene oxide (mlGO, 0.45 mg mL^{-1}) were prepared from the stock solutions obtained after synthesis (see the experimental details in ESM.S1† "*Synthesis of graphene oxide materials*") in deionized water. A 265.7 μM (100 μg mL^{-1}) stock solution of riboflavin was prepared in deionized water and diluted to 20 μM to prepared the working solution. The stock solution of riboflavin was prepared by sonication. The analytical procedure for GO determination was carried out as follows: 1 μM (0.38 μg mL^{-1}) of riboflavin was mixed with increasing concentrations of GO materials, at pH 7.5 fixed with 15 mM MES buffer. In this sense, 15 μL of riboflavin solution (7.5 μg mL^{-1}, 20 μM), 45 μL MES (0.1 M, pH 7.5) were mixed with GO aliquots of 240 μL of gradual concentrations (standards and samples), achieving a total volume of 300 μL. The mixtures were then vortexed and interacted for 3 min at room temperature to obtain the riboflavin–GO complex and measured. GO analyses were performed in the same way for all three materials. The fluorescence emission intensities of each sample in the absence (I_0) and presence (I) of GO (ml-, s- and lGO) were recorded at 524 nm, exciting at 368 nm. The fluorescence extinction efficiency of free riboflavin, expressed as (I_0/I), was used as analytical signal for GO determination.

To catechin determination, the concentration of riboflavin–lGO nanoplatform was constant and fixed to 1 μM of riboflavin and 126.1 μg mL^{-1} of lGO (corresponding to maximal quenched riboflavin signal). Specifically, to carry out these experiments 15 μL of riboflavin solution (7.5 μg mL^{-1}, 20 μM), 90 μL of lGO solution (0.42 mg mL^{-1}) and 45 μL MES (0.1 M, pH 6.5) were mixed with aliquots of 150 μL samples-containing different concentrations of catechin, to complete a total volume of 300 μL. Then, the mixtures were allowed to interact for 1 min at room temperature before measuring the emission signals at the same wavelength, exciting at 445 nm. The fluorescence recovery efficiency of free riboflavin, expressed as the ratio between the fluorescence of riboflavin–lGO complex in the presence (I) and absence (I_0) of catechin, was used as analytical signal.

Control experiments to verify that the switch-off-on of riboflavin emission was produced by the different affinities between the competitors (riboflavin and catechin) for GO were following the same protocol, replacing GO by deionized water.

Preparation of riboflavin–graphene oxide nanoplatform for characterization

FT-IR and Raman analyses were carried out to elucidate the possible interaction between riboflavin and GO to form the nanoplatform. The different complexes (1–3) were prepared by mixing 1 μM riboflavin with 126.1, 42.0 or 14.0 μg mL^{-1} of lGO, respectively. These solutions were fixed at pH 7.5 with 15 mM MES buffer solution. Each complex was prepared in triplicate.

Previously, a calibration curve of the free riboflavin emission signal at 524 nm (λ_{exc} 368 nm) was prepared between 0.05 and 1.00 μM. Once the previous samples were prepared, a control of them was followed by fluorescent measurements to quantify the free riboflavin. Excess free riboflavin in solution was removed from the complex by the necessary centrifugation processes at 10 000 rpm for 7 min. The supernatant was removed and the

complex was washed with deionized water. Depending on the complex, this process was repeated so many times until no free riboflavin was detected in the solution.

Finally, the samples were frozen by liquid nitrogen at −77 K and sublimated at 0.005 mbar for 3 days and were subjected to the characterization techniques.

Samples treatment

Waters of different origin and a soil were chosen as environmental samples for the determination of GO. To simulate samples of river, drinking, well and seawater contaminated with the nanomaterial, the environmental samples were fortified at four lGO concentration levels between 1.1 and 4.0 μg mL^{-1}. The same treatment was followed for all samples, including those of seawater. Thus, 2 mL of sample doped with each of the lGO concentrations were centrifuged for 7 min at 10 000 rpm. After that, 1.7 mL of the supernatant were carefully removed, remaining 300 μL of GO sample. Finally, after this pre-concentration step, samples were directly subjected to the analytical procedure previously described in section "*Analytical procedure for the analysis of GO and catechin*". In the case of soil samples, 0.3 g portions were spiked with different concentrations of lGO from 23.8 to 88.2 μg g^{-1} and left them to dry. Once the samples were dried, each of these portions was suspended in 1 mL of deionised water. This mixture was kept under continuous stirring for 5 min and subsequently allowed to settle until the supernatant was as clear as possible. Each obtained supernatant was subjected to the analytical procedure for the determination of lGO concentration. All samples were analysed in triplicate.

The determination of catechin was carried out in several food matrices, such as beverages (red wine and green tea) and cocoa beans. Different concentrations of catechin between 10.0 and 36.6 μg mL^{-1} were added to a liquid green tea sample, already prepared and bought in a local supermarket. This sample was previously 1 : 2 diluted with deionized water. 5 mL of spiked green tea were extracted with 2 mL diethyl ether to get rid of some unknown food additives. This extraction procedure was repeated three times. Finally, aqueous samples were subjected to the analytical process by triplicate.

The red wine sample was spiked at the same concentrations levels as the green tea. The treatment of this sample followed the sample procedure as for the tea samples, except that this sample was previously diluted 3 times.

On the other hand, roasted cocoa sample (Ocumare de la Costa, Venezuela) was treated as follows: the beans were crushed with a mortar until a uniform powder was obtained to achieve a better contact with the extractant mixture. 0.5 g of this powder were treated with 5 mL of an ethanol : water mixture (50 : 50, v/v), then sonicated for 20 min and, subsequently, the suspension was filtered through a cellulose membrane. The remaining cocoa powder was treated again with 5 mL of the extractant mixture, the suspension was then sonicated and finally filtered. Each one of the obtained extracts was directly subjected to the proposed analytical method and electrophoretic one (see the experimental conditions in ESM.S1† "*Quantification of catechin by capillary electrophoresis*") to estimate the catechin concentration in the sample. In addition, the cocoa sample was fortified at 2 concentration levels of catechin (30.24 and 69.72 μg g^{-1}) and the procedure was followed.

Results and discussion

Characterization of graphene oxide-based structures

Three graphene oxide-based structures with controlled lateral dimensions and thicknesses were synthesized by the Hummers procedure[28–30] (see the experimental details in ESM.S1† "*Synthesis of graphene oxide materials*"). Their physicochemical characteristics were exhaustively studied as detailed below. X-ray diffraction (XRD) analyses were carried out to elucidate the structural features of the synthesized materials. Graphitic materials always present a well-defined peak at 2θ ∼25–26° values characteristic of their (002) plane.[4] However, results of the synthesized graphene oxide-based materials plotted in Fig. S1A† do not show this specific plane, demonstrating their high purity after the oxidation treatment and change of hybridization. Small graphene oxide (sGO) and large graphene oxide (lGO) diffractograms show a peak related to the (001) plane at 2θ ∼11–12°. This shift in their 2θ values has already been reported because of water and oxygen functional groups incorporation between their layers after the oxidation procedure. In addition, this interlaminar space has previously been used to intercalate compounds for different applications, such as adsorption and catalysis.[5] Unlike lGO and sGO, no peak of any plane is clearly visible in the monolayer graphene oxide (mlGO) diffractogram, demonstrating its lack of crystalline character, and showing a more exfoliated and thinner structure in comparison to the other two materials.

Fig. S1B† compiles Raman results of the different materials. Typical and similar spectra have been detected. Two bands are distinguished between 1000 and 2000 cm^{-1}, the D-band at 1351 cm^{-1}, which describes the hybridized carbon disorder that is present in the GO, and the G-band located at 1598 cm^{-1} that is designated to sp^2-carbon atoms. The ratio between their intensities (I_D/I_G) has already been designated as a parameter to establish their degree of defects.[31] Based on D. López-Díaz classification,[32] these GOs can be considered as low-defected graphene based-materials because they exhibit I_D/I_G values between 0.90–0.91, $I_D/I_{G\text{-lGO}}\,(0.91) = I_D/I_{G\text{-sGO}}\,(0.91) \approx I_D/I_{G\text{-mlGO}}$ (0.90). In this sense, lGO and sGO display very similar results, being in agreement with F. Rodrigues *et al.* outcomes.[29] On the other hand, mlGO is characterized by a slightly less defected structure in comparison to the other two GOs.

Scanning transmission electron microscopy (STEM) experiments were carried out to define the morphology and size of the different GOs. Micrographs acquired are compiled in Fig. S1C.† Materials show defined flat structures typical of this kind of materials. The freeze-drying methodology used to dry the GO solution has permitted to obtain a less compacted material. Regarding the size of the materials, sGO flakes displays smaller (400–1200 nm) lateral dimensions than lGO (5–20 μm) and mlGO (5–25 μm). It has been seen that these materials have different thicknesses where that of sGO is 1.1–2.4 nm, that of lGO is 1.2–4.5 nm and that of mlGO is 0.6–0.9 nm.[30] This

suggests the monolayer structure of mlGO and multilayer ($n \geq 2$) of s- and lGO.

Fourier-transform infrared spectroscopy (FT-IR) was used to determine the surface chemistry of these materials. All of them present the same type of oxygen functional groups. Results are depicted in Fig. S1D.† They show a band centered at ~1725 cm^{-1} that is related to the stretching vibration of –C=O groups typically assigned to the existence of carboxylic groups. Fact that is verified by the presence of a shoulder at ~3612 cm^{-1} assigned to free hydroxyl groups.[33] In addition, a broad band from 2920 to 3620 cm^{-1} designated to –OH groups is also found. Additionally, the band centred at ~1620 cm^{-1} is related to the aromatic domain, sp^2 carbon, of the material that is connected with hydroxyl groups in acidic surfaces.[34] On the other hand, the change of hybridization is corroborated by the existence of a sharp band at 1065 cm^{-1}.[35] Finally, –C–H groups in aromatic structures can be established because of the existence of bands below 950 cm^{-1}.[36]

Fluorescence emission and UV-Vis absorbance results of the synthesized materials are plotted in Fig. S1E and S1F,† respectively. The main band of absorbance is located at 230 nm, which is characteristic of $\pi \rightarrow \pi^*$ transitions from sp^2 carbon domains. Additionally, a shoulder associated with $n \rightarrow \pi^*$ transitions of free electrons present in the oxygen atoms of their carbonyl and carboxyl surface functional groups, is visible at 300 nm.[37] Regarding the fluorescence emission results ranging from 370 to 570 nm, it can be seen that lGO and sGO display similar optical properties, however a bathochromic shift is found for mlGO.

Strategy for both GO and catechin detection

The novel sensor for the determination of GO and catechin that is proposed in this work is based on the competitive interactions between GO (host) and riboflavin or catechin (competing guests). Thus, this proposal is known as indicator displacement assay. Riboflavin was selected as fluorescent indicator, which displayed two excitation bands located at 368 and 445 nm and a strong emission signal at 524 nm (Fig. S2†). In contrast, GO and catechin spectra showed a very low emission at 524 nm even at high concentrations. Thus, these spectral contributions were not significant at the chosen excitation conditions. The emission band at 524 nm was monitored for indirectly sense GO and catechin based on a fluorescence turn-off-on effect. Both exciting wavelengths were selected to analyse the effect of both species over the riboflavin emission. Firstly, the adsorbent and the fluorescence quenching properties of the three-graphene oxide-based nanostructures (mlGO, sGO and lGO) towards riboflavin as dye probe, were evaluated. As shown in Fig. 1A, riboflavin fluorescence intensity was progressively decreasing as it interacts with increasing concentrations of all nanomaterials used,[1] allowing the GO sensing. The fluorescence intensity of riboflavin decreased dramatically as the GO concentration increased but then decreased more moderately at higher concentrations of GO, describing a polynomial fit for the three GO structures. This may be due to the higher number of active adsorption sites at the beginning of the process, which slows down as they are occupied. The efficiency of the quenching effect is more pronounced as GO concentrations increase (I_0/I). Specifically, the fluorescence of 1 μM riboflavin solution can be inhibited up to *ca.* 93% in the presence of 126.1 μg mL^{-1} lGO, which means that almost all indicator molecules are adsorbed onto the active sites of the nanolayers. Riboflavin fluorescence is not maximally inhibited because although the riboflavin–GO complex is being formed, there is probably a little dissociation of the complex leaving a small proportion of both free riboflavin and GO. Therefore, GO sensing is the result of indirectly measurements of the fluorescence of the remaining free riboflavin when forming the complex. Similar quenching profiles were observed in the case of l- and sGO, being different for mlGO (Fig. 1A). The slope of the fitting curve for the riboflavin and lGO is clearly the steepest one, so it can be concluded that the fluorescence quenching efficiency of the dye by GO materials follows the trend lGO > sGO > mlGO. This fact indicates that riboflavin shows a higher affinity for lGO to form the complex than with the rest of GO materials (the formation constant obtained for this complex will be higher than for the other materials). In view of these results, bigger and thicker

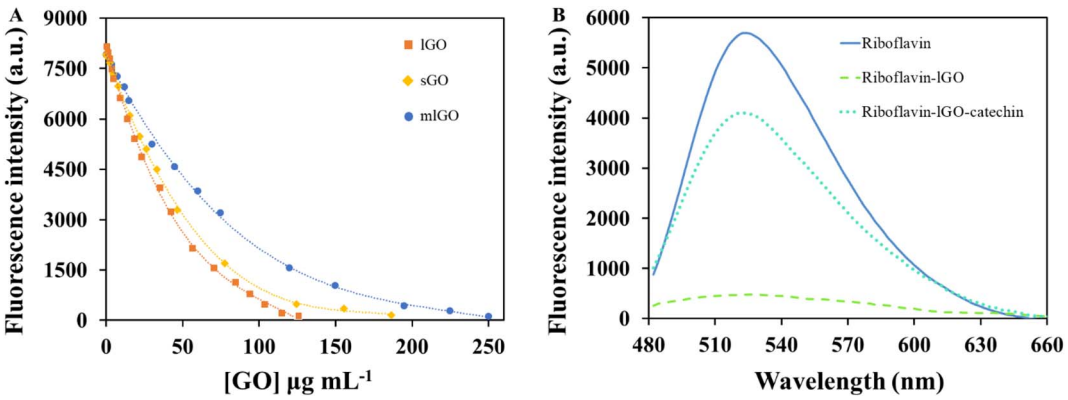

Fig. 1 (A) Effect of the GO types concentration on the riboflavin fluorescence to form riboflavin–GO systems. The solutions were prepared in 15 mM MES buffer at pH 7.5. Detection was performed at 524 nm (λ_{exc} 368 nm). (B) Fluorescence emission spectra of riboflavin in MES buffer solution at pH 6.5 under different conditions (λ_{exc} 445 nm, λ_{em} 524 nm). The concentration of each of the species was 0.4, 126.1 and 108.3 μg mL^{-1} for riboflavin, lGO and catechin, respectively.

flakes display an advantageous effect in comparison to the other GO materials for this fluorescence system. The inferiority on fluorescence quenching capacity of sGO with respect to lGO may be attributed to fewer sp^2 domains into sGO structure.[38] These results are in agreement with previous research based on the fluorescence quenching of small-molecule dyes by GO with different lateral size.[38,39] Thus, to achieve the maximum fluorescence inhibitory effect of 1 μM riboflavin solution, a higher concentration of nanomaterial is needed in the case of mlGO (249.8 μg mL^{-1}) than in the case of s- (186.4 μg mL^{-1}) or lGO (126.1 μg mL^{-1}). Therefore, for sensitivity reasons, lGO was selected to design the riboflavin-GO nanoplatform for the catechin sensing in the experimental conditions at which the presence of free riboflavin was not practically detectable. The consecutive addition of catechin to the previously formed riboflavin–GO complex led to a gradual recovery of the dye emission, as observed in Fig. 1B. The turn-on effect of the riboflavin fluorescence signal is related to the catechin amount added, suggesting another fluorescence approach for the detection of catechin *via* fluorescence indicator displacement assay. Thus, riboflavin, which in its free form presents a strong fluorescence, when it is attached to GO is turned-off and can re-ignite in the presence of catechin that releases it from the complex when forming the new riboflavin–GO–catechin system is formed. These results suggest the greater affinity of catechin for the GO surface in comparison to riboflavin. The maximum fluorescence of riboflavin that can be recovered was achieved in the presence of 108.3 μg mL^{-1} of catechin. The initial concentration of free riboflavin was 6.1×10^{17} molecules per mol, while 2.2×10^{20} molecules per mol of catechin were required to replace the maximum number of riboflavin molecules from the complex. It can be deduced that the release of riboflavin into solution in the presence of catechin is not in a 1 : 1 ratio. This may be logical since catechin molecules are structurally smaller than riboflavin, being more accessible to the GO active sites due to their less steric hindrance. Therefore, it is stablished that many catechin molecules are necessary to replace one of riboflavin. As can be seen in Fig. S3,† the capability of lGO to adsorb riboflavin decreases as the concentration of catechin present in the medium increases. This indicates the lower affinity of the material for riboflavin than for catechin. The fluorescent behavior observed by the developed procedure it is justified in this way, since there is a progressive increasing amount of free riboflavin to the solution. Thus, the new turn-on effect allows the sensing of catechin.

Furthermore, the effect of catechin on the emission of riboflavin was investigated (see ESM.S2 "*Evaluation of catechin effect over riboflavin fluorescence*" and Fig. S4†). Results revelated that there was a negligible effect on the riboflavin fluorescence intensity as the catechin concentration increases, demonstrating that there was no interaction between both compounds in the absence of GO flakes. Thus, it can be stated that the riboflavin fluorescence recovery was attributed to the replacement of riboflavin molecules for catechin ones on the surface of lGO to form a new complex catechin–GO, leaving riboflavin free in the solution and regaining its strong fluorescence as there is more catechin in the medium.

Optimization of experimental parameters for GO and catechin sensing

GO sensing. The performance of the proposed probe system to determine GO was affected by related factors including the pH, ionic strength, concentration of the indicator and the interaction time of the system. These factors were examined to obtain the highest sensitivity of the system. The first experimental variable studied that could influence the sensing of GO was the pH. The cationic form of riboflavin is non-fluorescent and the anionic form has a low fluorescence quantum yield. Only the neutral form of riboflavin is highly fluorescent.[40] Thus, the evaluated pH range was ranged between 3.5 and 8.0. The relationship between the fluorescence extinction efficiency, expressed as I_0/I (where I_0 and I are the riboflavin emission intensities in the absence and presence of GO, respectively) was used as analytical signal. The highest I_0/I signal ratio was found at pH 7.5 value. Fixing lower or higher pH values produced lower interaction between riboflavin and the GO-based nanomaterial (Fig. S5A†). Thus, pH 7.5, initially fixed with 25 mM MES as buffer, was selected for the following optimization parameters. Then, the ionic strength was evaluated, in the 5–40 mM range (Fig. S5B†). In this case, very insignificant differences (<3%) were observed between 15 and 25 mM. However, higher concentrations disfavoured the I_0/I ratio, as well as those below 10 mM. This behavior can be explained in terms of salting-in and salting-out effects.[41] In view of these results, it is not worth adding 25 mM of buffer if practically half of the concentration produces a similar effect. Therefore, 15 mM was selected as the minimum concentration of MES that implied the greatest interaction between riboflavin and GO. Also, riboflavin concentration from 0.5 to 10 μM was investigated (Fig. S5C†). A constant concentration of GO was established (47 μg mL^{-1}) to interact with the dye indicator. Then, the magnitude of the fluorescent extinction produced by the nanomaterial on the riboflavin emission intensity was tested. Results revealed that as the riboflavin concentration decreased, the I_0/I ratio considerably improved. The effect produced between concentrations from 10 to 2.5 μM was quite similar. The fixed GO concentration practically inhibits the 0.5 μM riboflavin fluorescence. However, concentrations below 1 μM of the probe emitted a rather noisy fluorescence signal. Therefore, and as a compromise between both factors, 1 μM was chosen as the lowest riboflavin concentration that presents a considerable fluorescent signal for a proper detection. In addition, the effect exerted by different GO structures was assessed under the previously selected conditions with multilayer and larger size GO, lGO. Defining the affinity between riboflavin and GO structure as the maximum quenching capacity, four concentration levels of GO were initially tested for each nanomaterial (ml-, s- and lGO), specifically 12, 24, 36 and 48 μg mL^{-1}. As shown in Fig. S5D,† at the lowest concentration of GO, similar quenching capacity was found for all of them. As the concentration of the quencher increased to 24 μg mL^{-1}, the fluorescence extinction efficiency was enhanced, being clearly maximum for multilayer GO materials. The greatest inhibition effect (I_0/I ratio) of riboflavin fluorescence was found with lGO at higher concentrations,

specifically from 36 μg mL^{-1}. This result could imply that the attractive interaction between riboflavin and lGO was stronger than sGO and mlGO. In all cases, the magnitude of the fluorescence quenching effect was dependent on the riboflavin–GO concentration ratio. The gradual improvement of the I_0/I signal with increasing GO concentrations was due to the existence of more active sites for riboflavin to get adsorbed, leading to a strong decrease of the fluorescence emission. Thus, lGO was selected as the material to perform the riboflavin–GO platform for the sensing of catechin.

A kinetic study between riboflavin and each GO structure was also carried out to test the interaction time needed to reach adsorption equilibrium (Fig. S6†). The maximal and constant analytical signal (I_0/I) was obtained in less than 3 min.

Catechin sensing. For the sensing of catechin, the riboflavin–lGO complex was firstly formed following the optimal conditions selected above until the maximal quenching of free riboflavin emission was achieved. It is important to avoid an excess of the adsorbent material since it can directly interact with catechin molecules. The maximal quenching effect of 0.38

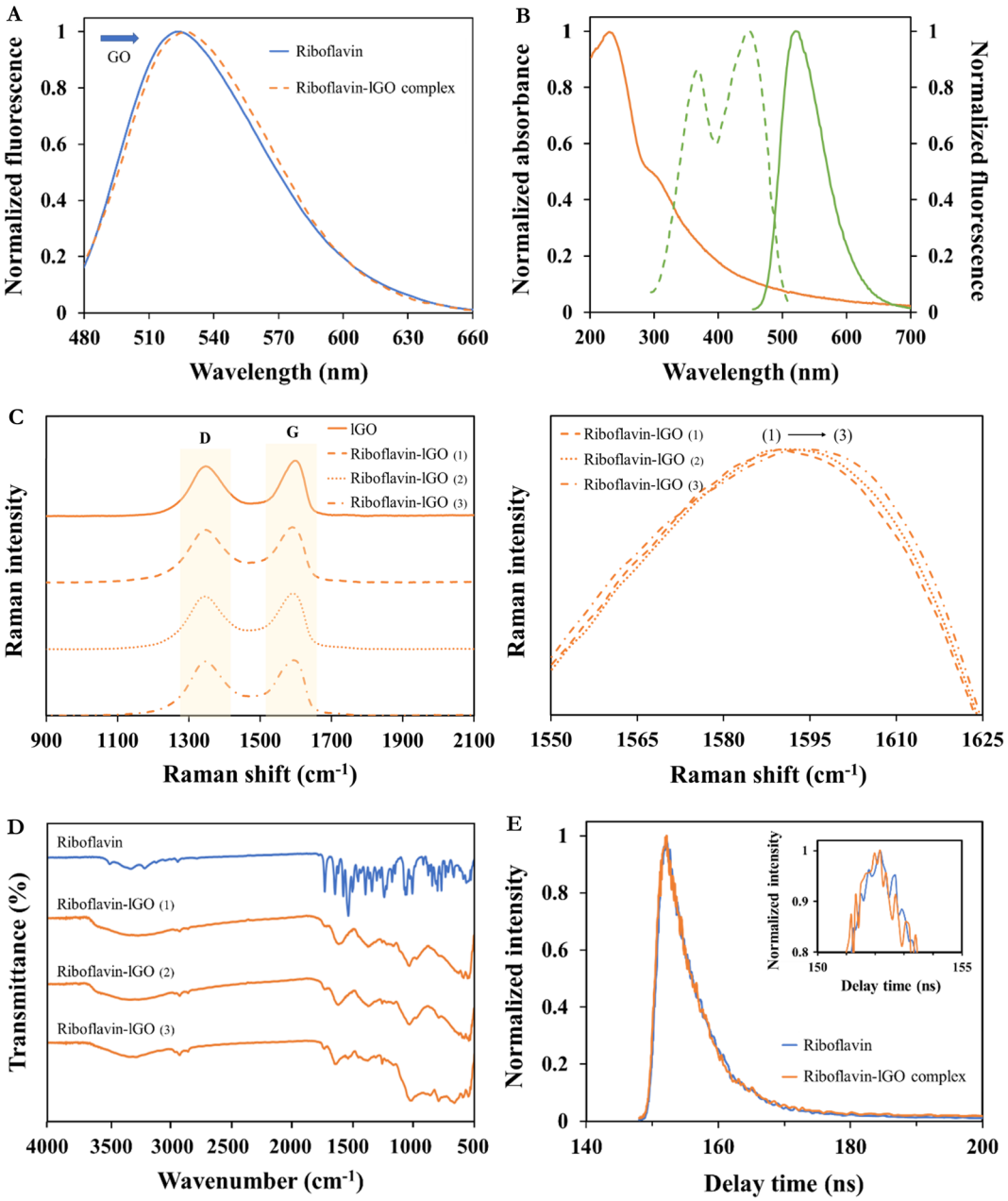

Fig. 2 Characterization of riboflavin–lGO nanoplatform. (A) Red-shift of riboflavin emission profile in the presence of 126.1 μg mL^{-1} lGO (complex formation). (B) Absorption spectrum of lGO (orange line) and fluorescence curves of riboflavin (excitation, green dotted line, and emission, green solid line). (C) Raman profiles of freeze-dried lGO and riboflavin–lGO complexes (1–3) from top to bottom (left). Extended spectrum area at the G-band position (right). (D) FT-IR profiles of the complexes. (E) Time-resolved fluorescence decays of riboflavin and riboflavin–lGO complex in a scanning range of 200 ns, under excitation at 368 nm and emission at 524 nm.

μg mL^{-1} free riboflavin solution was obtained with 126.1 μg mL^{-1} of lGO. Once riboflavin–lGO complex was formed at these experimental conditions, it was subsequently used as the nanoplatform for the sensing of catechin. Thus, several experimental variables that could affect the new sensing strategy, in terms of sensitivity and accuracy, were evaluated. In this case, the ratio between the fluorescence of riboflavin–lGO complex, namely free riboflavin emission intensity after being displaced from the complex, in the presence (I) and absence (I_0) of catechin, was used as analytical signal. The pH of the medium was examined in the 3.5–8.0 range (Fig. S5E†), although no relevant differences were found. Therefore, a pH of 6.5 value was fixed as the one that showed the highest analytical response. Subsequently, different concentrations of MES buffer between 5 and 30 mM were studied at pH 6.5 (Fig. S5F†). Once again, the results revealed that 15 mM was the optimal concentration for the sensing of catechin.

The interaction time required for the adsorption of catechin on lGO to occur was also investigated. As it can be observed in Fig. S7,† after 1 min of interaction the I/I_0 signal remains constant.

Characterization of riboflavin–graphene oxide nanoplatform and fluorescence mechanism

As previously shown, the fluorescence emission intensity of riboflavin was gradually decreased with increasing concentrations of GO. It is then demonstrated its potential as an effective nanoquencher and nanoadsorbent of riboflavin fluorophore. Furthermore, lGO did not present any fluorescence at the same excitation wavelength of riboflavin (λ_{exc} 368 nm), confirming that the observed extinction was due to the interaction with the dye and not the result of a reabsorption process.[6]

GO flakes mostly consist in hexagonal ring-based carbon system bearing sp^2 carbon atoms and many sp^3 carbons that hold the oxygen-containing functional moieties.[29] Therefore, GO structure would enable to accept electrons from donor compounds[42] being adsorbed on its surface probably *via* π–π stacking interactions. Steady-state emission profiles have demonstrated a strong quenching of riboflavin emission when they interact with GO. Furthermore, Fig. 2A shows a slight red shift in the maximum emission of the probe, between 524 and 528 nm. This effect is more promoted with the increment of lGO concentration from 0 to 126.1 μg mL^{-1}, showing that riboflavin molecules are strongly adsorbed at the lGO surface *via* π–π interactions.[6]

The fluorescence quenching of the excited-state riboflavin could take place by different possible processes, such as energy transfer or electron transfer. Fig. 2B shows that the emission spectrum of the fluorophore (riboflavin) does not overlap with the absorption band of the acceptor (GO), excluding the possibility of the energy transfer process between both compounds to occur.[43] Therefore, the quenching effect that is plausible to occur follows an electronic transfer process.[44] The same behaviour on naphthylamide dye with GO was previously reported by Seraj and Rouhani[6] and on rhodamine B, eosin and methylene blue with graphite oxide and graphene was reported by Liu *et al.*[44]

To confirm the possible interaction between riboflavin dye and the lGO surface, Raman and FT-IR analyses of the different riboflavin–GO complexes (1–3) at different concentrations (126.1, 42.0 and 14.0 of lGO μg mL^{-1}, respectively) were carried out.

I_D/I_G results show the greatest disorder degree for the complex with more riboflavin adsorbed (I_D/I_G = 0.98). Earlier publications have also demonstrated the use of Raman spectroscopy as a tool to define the way that different molecules and carbon-based materials interact.[45,46] Thus, the Raman shift values of their G band are compiled and shown in Fig. 2C and Table S1.† In this sense, results obtained from these riboflavin–lGO complexes corroborate our previous fluorescence outcomes, since the graphitic-sp^2 (G) band of the different complexes shows a visible shift, being maximum for the highest I_D/I_G value. In contrast, an alteration in the D-band shift between complexes has not been observed.

FT-IR technique has previously been used as a tool to help elucidating the possible interactions between organic molecules and solid surfaces. In this case, Fig. 2D shows the spectrum of the riboflavin dye and its composites formed with the lGO solutions (riboflavin–lGO). The riboflavin spectrum displays two main contributions of –OH functional groups at 3315 and 1240 cm^{-1}. Aliphatic groups are detected by bands at 2932 and 2850 cm^{-1}. The band centred at 1727 cm^{-1} is attributed to –C═O stretching vibration of the isoalloxazine ring. Also, the band assigned to the ring –C═N stretching vibration is found at 1644 cm^{-1} and the band at 1534 cm^{-1} can be assigned to –C═C– group. Additionally, the band at 1062 cm^{-1} is correlated with –C═O stretching vibrations. The lGO complexes present representative bands of the dye, proving its presence on the surface of the material. These bands are more pronounced for the riboflavin–lGO (3) complex. The complexes do not show any new band in respect to the initial lGO spectrum (Fig. S1D†), revealing that covalent interactions can be ruled out. These findings support previous Raman and fluorescence spectroscopy results, showing that hydrophobic or π–π interactions could be the main driving forces for lGO–riboflavin complexes.

The species used in this study are in solution, which means that there is a high possibility of interactions to be produced between the fluorophore and the fluorescence extinctor. The processes by which the observed quenching effect can occur are diverse, such as reactions of excited states, energy transfer, complex formation and collision quenching.[47] The molecular contact between the fluorophore and quencher is the responsible for the deactivation of the fluorescent emission. The quenching constant obtained by the Stern–Volmer equation (K_{SV}) indicates the sensitivity of the fluorophore to the deactivator. Greater K_{SV} values promote higher accessibility of one specie to the other.[47] As it will be discussed below, K_{SV} values obtained for riboflavin–lGO system are considerably higher than riboflavin–sGO and riboflavin–mlGO systems. This fact confirms that favourable interactions between lGO sheets and riboflavin molecules are obtained, enhancing the quenching efficiency of GO.[38] To evaluate the type of quenching mechanism that the developed procedure follows, the measurements

of lifetime for riboflavin and riboflavin–lGO system were defined.[48,49]

Generally, fluorescence decay can give information related to the excited-state of the fluorophore, being very useful to study the energy transfer- or electron transfer-induced fluorescence quenching. The lifetime values of the riboflavin and riboflavin–lGO complex were calculated by fitting the decay profiles with one-exponential, resulting in 5.70 ± 0.06 ns (100% ± 1.1) and 5.23 ± 0.05 ns (100% ± 1.6), respectively. The obtained values of χ^2 for both decays were 1.01 and 1.07, close to 1, which indicates the perfection fitting of the curve. These short lifetimes differentiate the fluorescence process from another well-known luminous phenomenon, such as phosphorescence. The molecular contact between species can be produced by two processes: (i) a *static quenching*, which is based on the formation of a non-fluorescent ground-state complex and (ii) the *dynamic quenching*, which is a result from the collisions between the quencher agent and fluorophore during the excited state. This last one produces a rapid recovery to its ground-state without the emission of a photon. In the case of a *static quenching*, the fluorescence lifetime of the fluorophore should not change in the presence of the quencher.[50] As shown in Fig. 2E, the fluorescence lifetime obtained for riboflavin was almost unchanged in the presence of lGO suggesting that the fluorescence change of riboflavin did not follow the to the excited state perturbation.[51] Thus, it can be concluded that the occurred effect is mainly referred to as *static quenching* mechanism in which the dye and GO forms a non-fluorescent complex at ground-state,[47,52] being the *dynamic quenching* little significant in the conditions in which the study was carried out.

The value of the binding constant (K_s) for the formation of the riboflavin–lGO complex and the number of binding sites (n) of the nanomaterial are 1.51 × 10^{-3} mL μg^{-1} and 1.79 (~2), respectively.[48,49] These results were obtained by the steady-state fluorescence measurements.

As revealed by fluorescence studies, there is greater affinity of catechin for the adsorbent material (lGO) compared to riboflavin, which is attributed to the size difference and the hydrophilic character. Catechin molecules display smaller size than those of riboflavin, being more accessible to interact with the active centers of GO. In addition, catechin has a lower hydrophilic character than riboflavin due to its higher aromaticity, being this characteristic more favorable for the interaction with GO.

Analytical performance characteristics

Several analytical performance characteristics were evaluated to examine the possible applicability of the proposed analytical procedure for both GO and catechin detection.

As previously mentioned, the fluorescence extinction of riboflavin as dye indicator with increasing concentrations of the different GO structures can be used for quantitative determination of GO. Fig. 3A shows a clear linear relationship between the riboflavin fluorescence ratio in the absence (I_0) and presence (I) of lGO concentrations from 0.6 to 35.4 μg mL^{-1}. Stern–Volmer plot of this phenomenon resulted to be I_0/I = 0.843 + 0.026 × [lGO] (μg mL^{-1}) with a determination coefficient of 0.996. For sGO and mlGO, a good linear dependence was also found when plotting the analytical signal (I_0/I) and the GO concentration. The precision of the proposed method for GO determination was evaluated in terms of repeatability and reproducibility expressed as relative standard deviation (RSD), both as function of concentration and (I_0/I) signal. For determining the repeatability, ten independent measurements of lGO standard solutions were carried out consecutively at 14 μg mL^{-1}. RSD values (intra-day conditions, n = 10) were 5.2% as function of concentration and 1.6% as function of I_0/I signal. For reproducibility test (inter-day conditions, n = 5), RSD values of 6.7% and 2.1% were found for lGO as function of concentration and I_0/I signal, respectively. The sensitivity of the proposed analytical procedure was assessed in terms of limit of detection (LOD) and quantification (LOQ). The LOD value found for lGO was 0.2 μg mL^{-1}, which was experimentally calculated. Table 1 also summarizes the details of the analytical figures of merits for the determination of sGO and mlGO materials. According to the slopes of each of the linear fits (K_{SV}), the higher

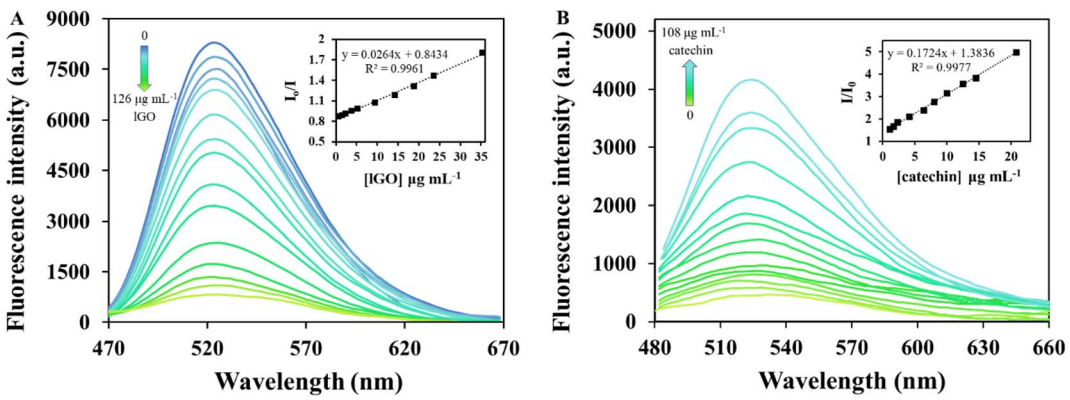

Fig. 3 (A) Calibration curve of lGO. The concentration of riboflavin was 0.38 μg mL^{-1}, pH 7.5, 15 mmol L^{-1} MES. The insets show the plots of the fluorescence extinction efficiency (I_0/I, λ_{exc} = 368 nm, λ_{em} = 524 nm) against the concentration each of the GOs. (B) Calibration curve of catechin. The concentration of riboflavin was 0.38 μg mL^{-1}, 126.1 μg mL^{-1} lGO, pH 6.5, 15 mmol L^{-1} MES. The inset shows the fluorescence recovery efficiency (I/I_0, λ_{exc} = 445 nm, λ_{em} = 524 nm) plotted against the catechin concentration.

Table 1 Analytical figures of merits of the proposed methodology for the quantification of GO materials and (+)-catechin

Analyte	Regression equation	Linear range (μg mL^{-1})	LOD (μg mL^{-1})	LOQ (μg mL^{-1})	R^2	$S_{y/x}$	RSD% intra-day[a]		RSD% inter-day[b]	
							Concentration	I_0/I	Concentration	I_0/I
lGO	$I_0/I = (0.026 \pm 0.001)$[lGO] + (0.843 ± 0.009)	0.6–35.4	0.2	0.6	0.996	0.020	5.2	1.6	6.7	2.1
sGO	$I_0/I = (0.023 \pm 0.001)$[sGO] + (0.967 ± 0.013)	1.2–33.2	0.4	1.2	0.994	0.023	6.5	1.5	8.4	1.9
mlGO	$I_0/I = (0.018 \pm 0.001)$[mlGO] + (0.946 ± 0.013)	3.8–60.1	1.3	3.8	0.997	0.023	5.6	1.9	8.8	2.5
Catechin	$I/I_0 = (0.172 \pm 0.003)$[catechin] + (1.384 ± 0.030)	1.0–20.8	0.2	1.0	0.998	0.056	3.1	1.2	5.8	2.3

[a] Measurements under intra-day conditions with $n = 10$ for GO materials and $n = 15$ for catechin. To evaluate RSD of the method, 14 μg mL^{-1} were used in the case of lGO and sGO; 30 μg mL^{-1} for mlGO and 14 μg mL^{-1} for catechin. [b] Measurements under inter-day conditions with $n = 5$ both for GO materials and catechin.

affinity of riboflavin for lGO (0.026 mL μg^{-1}) than for sGO (0.023 mL μg^{-1}) and for mlGO (0.018 mL μg^{-1}) is noteworthy, confirming all the above. The quenching magnitude (the slope of the fitting curves) is higher than those previously reported for similar species involved in this effect.[53]

To further evaluate the performance of the riboflavin-lGO probe system for catechin detection, the fluorescence signal of free riboflavin (displaced from the complex) was investigated at different catechin concentrations under the optimized conditions. As shown in Fig. 3B, the probe system gradually begins to fluoresce again as the catechin concentration increased. In the wide range of catechin concentrations evaluated (0.2–125.1 μg mL^{-1}), a first linear range with a steeper slope that comprised concentrations between 1.0 and 20.8 μg mL^{-1} and a coefficient of determination of 0.998 was found. The fluorescence recovery efficiency of riboflavin in the presence and absence of catechin (I/I_0) against the target analyte concentrations is represented in Fig. 3B inset. Meanwhile, for concentrations that exceeded 20.8 μg mL^{-1} and up to 108.3 μg mL^{-1}, a second linear response with a lower slope was observed with a value of 0.993 as determination coefficient. Being a stronger competitor, initially at lower catechin concentrations it should be easier for riboflavin to be released from the complex, hence the difference in slopes. Concentrations higher than 108.3 μg mL^{-1} did not produce further fluorescence recovery. As is recommended to work in the first linear range of concentrations, the quantification of the samples was carried out in this region. The regression equation of the first linear fit was $I/I_0 = 1.384 + 0.172 \times$ [catechin] (μg mL^{-1}). The sensing platform begins to recognize catechin at 0.2 μg mL^{-1}, therefore this value was considered as the experimentally calculated LOD. Concentrations between 0.2 and 1.0 μg mL^{-1} were perfectly detected but not quantifiable. In this case, the repeatability (intra-day conditions) was evaluated though fifteen analyses of 14 μg mL^{-1} standard solution and an RSD value of 3.1% in concentration terms was found. Reproducibility (inter-day conditions) was evaluated by quintuplicate at the same catechin concentration, obtaining an RSD value of 5.8%. These results suggest that the fluorescence probe system can be easily applied for the quantitative determination of catechin and with good sensitivity.

The details corresponding to the analytical figures of merits for both sensing systems are summarized in Table 1. It should be noted that the proposed sensing systems, both for the detection of GO and catechin, have attractive qualities such as their sensitivity, the simplicity of the analysis in a very short time and are relatively environmentally friendly sensors (employing a vitamin as sensor probe). This analysis strategy allows simultaneous detection and offers a new approach to sensing other compounds of the same nature.

The selectivity study of the proposed method was carried out by means of an interference test whose results appear in ESM.S2 and Fig. S8.†

Analytical applications

Although there are more and more analytical techniques and methods available for the detection, characterization and

Table 2 Recoveries obtained in environmental enriched samples with lGO

Determination of lGO					
Type of sample	Sample	Spiked concentration	Found concentration[a]	Recovery ($n = 3$, %)	RSD ($n = 3$, %)
River water (μg mL^{-1})	1	1.05	1.02 ± 0.03	97.1 ± 2.9	3.0
	2	1.89	1.82 ± 0.05	96.0 ± 2.7	2.8
	3	2.94	2.92 ± 0.09	99.2 ± 3.0	3.0
	4	3.99	4.01 ± 0.12	100.5 ± 2.9	3.1
Well water (μg mL^{-1})	1	1.05	1.05 ± 0.03	99.8 ± 3.2	3.2
	2	1.89	1.82 ± 0.06	96.2 ± 3.0	3.1
	3	2.94	2.85 ± 0.08	97.1 ± 2.7	2.8
	4	3.99	3.86 ± 0.13	96.8 ± 3.2	3.3
Drinking water (μg mL^{-1})	1	1.05	1.07 ± 0.03	101.8 ± 2.8	2.7
	2	1.89	1.84 ± 0.05	97.3 ± 2.5	2.5
	3	2.94	2.91 ± 0.08	99.1 ± 2.7	2.7
	4	3.99	3.93 ± 0.11	98.5 ± 2.8	2.9
Seawater (μg mL^{-1})	1	1.05	1.04 ± 0.03	98.8 ± 3.1	3.2
	2	1.89	1.84 ± 0.05	97.1 ± 2.5	2.6
	3	2.94	3.02 ± 0.08	102.6 ± 2.8	2.7
	4	3.99	4.00 ± 0.12	100.2 ± 3.1	3.1
Soil (μg g^{-1})	1	23.80	23.54 ± 0.73	98.9 ± 3.0	3.1
	2	40.25	39.97 ± 1.01	98.4 ± 2.5	2.5
	3	64.40	62.65 ± 2.29	97.3 ± 3.6	3.7
	4	88.20	86.17 ± 2.68	97.7 ± 3.0	3.1

[a] Average of 3 independent spiked samples ± standard deviation.

quantification of nanomaterials, although they are still scarce, their application to complex samples is still very limited and they are far from being incorporated into routine analysis.

The usefulness of the developed sensing strategy for GO analysis was proved by its application to different environmental samples (waters from different nature and a soil) and in the case of catechin, food samples (cocoa beans and beverages) were used. Each sample was treated according to the procedure already described in section "*Samples treatment*" and subsequently submitted to the analytical procedure detailed in section "*Analytical procedure for the analysis of GO and catechin*". All samples were analysed in triplicate by the proposed fluorometric assay.

The different water samples were fortified at four concentration levels of lGO between 1.1 and 4.0 μg mL^{-1} and the soil sample was also doped with the nanomaterial in the range 23.8–88.2 μg g^{-1}. Previously, all the matrices were checked not showing interference in the analytical signal. The concentration of lGO in each sample was estimated by external calibration and the obtained results are summarized in Table 2. As can be observed, satisfactory results were obtained for all of them with recovery values of the added GO between 96 and 103% and from 97 to 99% for water and soil samples, respectively. Furthermore, RSD values ($n = 3$) were lower than 4% for all environmental samples evaluated. The fluorescence turn-off effect produced by

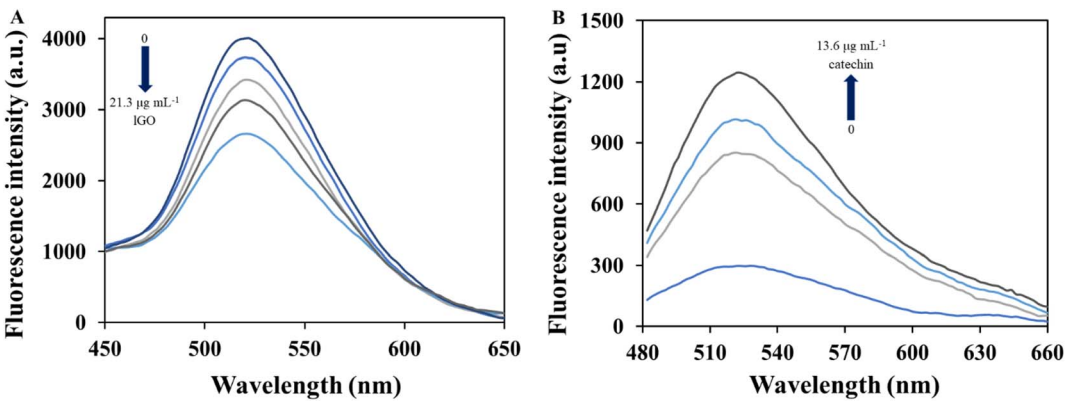

Fig. 4 (A) Analysis of a well water sample fortified at different concentration levels of lGO between 1.1 and 4.0 μg mL^{-1}. The concentration of riboflavin was 0.38 μg mL^{-1}, 15 mmol L^{-1} MES, pH 7.5, 3 min interaction time, λ_{exc} 368 nm and λ_{em} 524 nm. (B) Detection of catechin in a cocoa sample containing the analyte endogenously and after adding 3.0 and 7.0 μg mL^{-1}. The concentration on riboflavin was 0.38 μg mL^{-1}, 126 μg mL^{-1} lGO, 15 mmol L^{-1} MES, pH 6.5, 1 min interaction time, λ_{exc} 445 nm and λ_{em} 524 nm.

Table 3 Recoveries obtained in food matrices enriched with catechin

Determination of (+)-catechin					
Type of sample	Sample	Spiked concentration	Found concentration[a]	Recovery ($n = 3$, %)	RSD ($n = 3$, %)
Red wine (μg mL^{-1})	1	10.00	9.92 ± 0.32	99.2 ± 3.2	3.2
	2	18.32	18.15 ± 0.55	99.1 ± 3.0	3.0
	3	25.00	24.48 ± 0.68	97.9 ± 2.7	2.8
	4	36.60	34.97 ± 1.05	95.6 ± 2.9	3.0
Green tea (μg mL^{-1})	1	10.00	10.19 ± 0.34	101.9 ± 3.4	3.3
	2	18.32	18.25 ± 0.51	99.6 ± 2.8	2.8
	3	25.00	23.76 ± 0.77	95.0 ± 3.1	3.2
	4	36.60	34.47 ± 1.28	94.2 ± 3.5	3.7

[a] Average of 3 independent spiked samples ± standard deviation.

Table 4 Determination of catechin in cocoa beans using the proposed fluorescence methodology and CE-DAD method. Recoveries obtained in cocoa beans enriched sample

	Original amount					
Sample	CE-DAD ($n = 5$)	This method ($n = 5$)	Spiked concentration	Found concentration	Recovery ($n = 3$, %)	RSD ($n = 3$, %)
Cocoa beans (μg g^{-1})	92.4 ± 4.3	103.5 ± 3.3	30.24	131.37 ± 4.20	98.3 ± 3.1	3.2
			69.72	170.07 ± 5.96	98.2 ± 3.4	3.5

lGO in well water matrix can be seen in Fig. 4A and that produced in the other environmental samples can be observed in Fig. S9.† In Fig. S9C,† it can be appreciated a lower fluorescence of the probe in the presence of seawater matrix (blank assay) compared to that observed for other water matrixes, probably due its higher salinity. However, the high ionic strength of the sample does not affect the gradual response of the analytical signal in the presence of increasing concentrations of the analyte to be detected. Therefore, this aspect is not an issue and this sample was not been pre-treated before analysis.

On the other hand, the determination of catechin in liquid food samples was carried out by adding the target analyte to a green tea and a red wine sample in the concentration range 10.0–36.6 μg mL^{-1}. In this case and for both types of samples, an alteration in the analytical signal was observed by the corresponding matrix. As can be observed in Table 3, the recovery values obtained were quite favorable for both types of samples, especially for those with lower concentrations of catechin. At higher concentrations of this analyte in the sample, the catechin concentrations found are increasingly lower than the added ones. This may be since other compounds present in the matrix have a slight affinity to the riboflavin–GO complex and can be adsorbed, competing with catechin molecules (possible interferers). Even so, recovery values between 95 and 99% were found for red wine samples and for green tea ones were between 94 and 102% with low RSD values (≤4%) for all of them. Fig. S10† shows the turn-on effect produced in the red wine and green tea samples.

In both GO and catechin sensing (Fig. S9 and S10†), a blank assay was always performed to evaluate the effect of the matrix on the fluorescent signal obtained. Thus, if there is a matrix effect, it can be easily subtracted.

The determination of catechin was also performed in a cocoa beans sample, which endogenously contains the analyte. Moreover, cocoa beans sample was spiked at two concentration levels of catechin. Recovery values were around 98% as summarized in Table 4, which ensures the accuracy of the proposed method. Fig. 4B presents the results found for the determination of catechin in the cocoa matrix by the proposed procedure. As a further validation study and with the aim to prove the reliability of the proposed catechin sensor, the cocoa sample was also submitted to a previously validated electrophoretic method,[27] slightly modified, to estimate the flavonoid concentration. The analyses were performed by five-fold. The experimental conditions of the modified electrophoretic method appear in section ESM.S1† "*Quantification of catechin by capillary electrophoresis*". The analyses were performed by five-fold and Table 4 summarizes the obtained concentration values of catechin in cocoa sample by the proposed fluorometric procedure and the capillary electrophoresis (CE) method. Once the cocoa results were obtained, Student-*t* test was performed between these two sets of data to verify the statistical accordance between the results found by both methodologies.[54] The values for t_{exp} and t_{crit} were 1.0 and 2.8, respectively. As the value of t_{exp} is lower than that of t_{crit}, the absence of significant differences between the results obtained by both methodologies can be guaranteed, which would prove its comparative accuracy at the checked level of confidence (95%). These results demonstrated the potential applicability of the fluorometric probing system for the detection of catechin in cocoa samples, even in the presence of other co-existing compounds in the same matrix. The difference between the analysis time required

for each of the procedures should be highlighted, being much shorter, in the order of 10 times, for the fluorometric sensor.

Conclusions

In this study, a competitive adsorption–desorption behaviour of a popular fluorescent vitamin and a flavonoid compound, riboflavin and catechin, on a chemically heterogeneous GO surface is discussed in this study. Thus, a novel and label-free turn-off-on fluorescent approach for the detection of both, GO and catechin, based on the riboflavin–GO and catechin–GO complexes formation was developed.

Herein, riboflavin emission was gradually turned-off as the fluorophore interacted with GO flakes by π–π stacking interactions. The strongest interaction was produced between the dye and lGO, followed by sGO and lastly with mlGO. Therefore, the former was selected based on the least amount of nanomaterial needed for the complex production and the highest quenching effect. In this sense, it has been stablished that the lateral size and the thickness of these carbon-based nanostructures are very important physicochemical parameters for the good performance of this type of novel sensors. This effect occurred for the three GO types evaluated, allowing the quantitative analysis of this type of nanomaterial. Detection limits of GO structures were 0.2, 0.4 and 1.3 μg mL^{-1}, for lGO, sGO and mlGO, respectively. Once the riboflavin-GO complex was formed at the maximum fluorescence extinction, the presence of catechin (as stronger competitor) was capable to replace riboflavin (as weaker competitor) from the complex, switching-on the fluorescence signal due to the competitive adsorption between catechin and riboflavin for the GO active sites. Catechin quantification range was wide from 1.0 to 20.8 μg mL^{-1} and the limit of detection resulted to be 0.2 μg mL^{-1}. Compared to traditional instrumentation (HPLC, GC, or CE) for catechin analysis, the advantage of this developed procedure was based on short analysis times, economy, easy to operate, no tedious sample pre-treatment required, and to be an eco-friendly strategy. The novel developed sensor was also applied to real samples with satisfactory results, demonstrating its potential applicability. This dual determination significantly contributes to the first (GO as analyte) and second (GO as nanotool) way of Analytical Nanoscience and Nanotechnology.

Furthermore, the detection platform is a potential assay principle for the detection of other interesting organic molecules and biomolecules due to the different adsorption capacity of multiple fluorophores and analytes with different molecular structures.

Author contributions

Analytical chemistry section. Esther Pinilla-Peñalver: conceptualization, formal analysis, data curation, methodology, investigation, writing – original draft, writing – review & editing, visualization. Ana M. Contento: investigation, methodology, supervision, writing – review & editing. Ángel Ríos: investigation, conceptualization, writing – review & editing, supervision, funding acquisition, project administration. Material science section. Adrián Esteban-Arranz: investigation, methodology, writing – review & editing.

Conflicts of interest

There are no conflicts to declare.

Acknowledgements

The Spanish Ministry of Science and Innovation (MICINN) and Regional Government of Castilla-La Mancha (JCCM) are gratefully acknowledged for funding this investigation with Grants PID2022-138761NB-I00 and SBPLY/21/180501/000188, respectively. E. Pinilla-Peñalver also acknowledges MINECO for the predoctoral contract BES-2017-080357. We also want to thank E. Prado for the STEM measurements and M. C. Carrión for the Raman experiments.

References

1 G. Li, C. Xu, H. Xu, L. Gan, K. Sun and B. Yuan, Tunable graphene oxide for the low-fouling electrochemical sensing of uric acid in human serum, *Analyst*, 2023, **148**, 2553–2563, DOI: 10.1039/d3an00291h.

2 P. Zheng and N. Wu, Fluorescence and sensing applications of graphene oxide and graphene quantum dots: a Review, *Chem.–Asian J.*, 2017, **12**(18), 2343–2353, DOI: 10.1002/asia.201700814.

3 D. G. Jr Goodwin, A. S. Adeleye, L. Sung, K. T. Ho, R. M. Burgess and E. J. Petersen, Detection and quantification of graphene-family nanomaterials in the environment, *Environ. Sci. Technol.*, 2018, **52**(8), 4491–4513, DOI: 10.1021/acs.est.7b04938.

4 A. Esteban-Arranz, M. Pérez-Cadenas, V. Muñoz-Andrés and A. Guerrero-Ruíz, Evaluation of graphenic and graphitic materials on the adsorption of Triton X-100 from aqueous solution, *Environ. Pollut.*, 2021, **284**, 117161–117170, DOI: 10.1016/j.envpol.2021.117161.

5 A. Esteban-Arranz, D. Compte-Tordesillas, V. Muñoz-Andrés, M. Pérez-Cadenas and A. Guerrero-Ruíz, Effect of surface, structural and textural properties of graphenic materials over cooperative and synergetic adsorptions of two chloroaromatic compounds from aqueous solution, *Catal. Today*, 2018, **301**, 104–111, DOI: 10.1016/j.cattod.2017.03.048.

6 S. Seraj and S. Rouhani, Fluorescence quenching as an efficient tool for sensing application: study on the fluorescence quenching of naphthalimide dye by graphene oxide, *Int. J. Chem. Mol. Eng.*, 2018, **11**(12), 851–854, DOI: 10.5281/zenodo.1316855.

7 E. Bozkurt, M. Acar, Y. Onganer and K. Meral, Rhodamine 101–graphene oxide composites in aqueous solution: the fluorescence quenching process of rhodamine 101, *Phys. Chem. Chem. Phys.*, 2014, **16**(34), 18276–18281, DOI: 10.1039/C4CP01492H.

8 S. T. Huang, Y. Shi, N. B. Li and H. Q. Luo, Sensitive turn-on fluorescent detection of tartrazine based on fluorescence

resonance energy transfer, *Chem. Commun.*, 2012, **48**(5), 747–749, DOI: 10.1039/C1CC15959C.

9 C. P. Li, S. Tan, H. Ye J. Cao and H. Zhao, A novel fluorescence assay for resveratrol determination in red wine based on competitive host-guest recognition, *Food Chem.*, 2019, **283**, 191–198, DOI: 10.1016/j.foodchem.2018.12.133.

10 R. Martín-Folgar, A. Esteban-Arranz, V. Negri and M. Morales, Toxicological effects of three different types of highly pure graphene oxide in the midge Chironomus riparius, *Sci. Total Environ.*, 2022, **815**, 152465–152474, DOI: 10.1016/j.scitotenv.2021.152465.

11 S. Benítez-Martínez, A. I. López-Lorente and M. Valcárcel, Graphene quantum dots sensor for the determination of graphene oxide in environmental water samples, *Anal. Chem.*, 2014, **86**(24), 12279–12284, DOI: 10.1021/ac5035083.

12 F. A. Monikh, L. Chupani, M. G. Vijver, M. Vancová and W. J. Peijnenburg, Analytical approaches for characterizing and quantifying engineered nanoparticles in biological matrices from an (eco) toxicological perspective: old challenges, new methods and techniques, *Sci. Total Environ.*, 2019, **660**, 1283–1293, DOI: 10.1016/j.scitotenv.2019.01.105.

13 E. Pinilla-Peñalver, M. J. Villaseñor and A. M. Contento, Á. Ríos. Erythrosine B–coated gold nanoparticles as an analytical sensing tool for the proper determination of both compounds based on surface-enhanced Raman spectroscopy, *Microchem. J.*, 2020, **157**, 104937–104948, DOI: 10.1016/j.microc.2020.104937.

14 C. Suárez-Oubiña, P. Herbello-Hermelo, P. Bermejo-Barrera and A. Moreda-Piñeiro, Single-particle inductively coupled plasma mass spectrometry using ammonia reaction gas as a reliable and free-interference determination of metallic nanoparticles, *Talanta*, 2022, **242**, 123286–123295, DOI: 10.1016/j.talanta.2022.123286.

15 S. Yang, Q. Chen, M. Shi, Q. Zhang, S. Lan, T. Maimaiti, Q. Li, P. Ouyang, K. Tang and S. T. Yang, Fast identification and quantification of graphene oxide in aqueous environment by Raman spectroscopy, *Nanomaterials*, 2020, **10**(4), 770–780, DOI: 10.3390/nano10040770.

16 A. Cayuela, M. L. Soriano and M. Valcárcel, β-Cyclodextrin functionalized carbon quantum dots as sensors for determination of water-soluble C 60 fullerenes in water, *Analyst*, 2016, **141**(9), 2682–2687, DOI: 10.1039/C5AN01910A.

17 E. Pinilla-Peñalver, M. L. Soriano, G. M. Durán, E. J. Llorent-Martínez, A. M. Contento and Á. Ríos, Discrimination between nanocurcumin and free curcumin using graphene quantum dots as a selective fluorescence probe, *Microchim. Acta*, 2020, **187**(8), 1–11, DOI: 10.1007/s00604-020-04437-x.

18 C. Montes, M. L. Soriano, M. J. Villaseñor and Á. Ríos, Design of a 3D interfacial sers liquid sensing platform based on Au-nanobones for discrimination and quantitation of quercetin loaded nanoemulsions, *Sens. Actuators, B*, 2022, **358**, 131509–131519, DOI: 10.1016/j.snb.2022.131509.

19 N. Maheshwari and R. Mahmood, Protective effect of catechin on pentachlorophenol-induced cytotoxicity and genotoxicity in isolated human blood cells, *Environ. Sci. Pollut. Res.*, 2020, **27**(12), 1–18, DOI: 10.1007/s11356-020-07969-0.

20 H. Mechchate, I. Es-Safi, H. Haddad, H. Bekkari, A. Grafov and D. Bousta, Combination of catechin, epicatechin, and rutin: optimization of a novel complete antidiabetic formulation using a mixture design approach, *J. Nutr. Biochem.*, 2021, **88**, 108520–108537, DOI: 10.1016/j.jnutbio.2020.108520.

21 S. Dutta, S. Priyadarshini, J. A. Moses and C. Anandharamakrishnan, Supercritical Fluid and Ultrasound-assisted Green Extraction Technologies for Catechin Recovery, *ChemBioEng Rev.*, 2021, **8**(6), 654–664, DOI: 10.1002/cben.202100001.

22 C. Du, C. Ma, J. Gu, L. Li, C. Zhu, L. Chen, T. Wang and G. Chen, Rapid Determination of catechin content in black tea by fluorescence spectroscopy, *J. Spectrosc.*, 2020, **2020**, 1–8, DOI: 10.1155/2020/2479612.

23 A. Larrauri, O. Núñez, S. Hernández-Cassou and J. Saurina, Determination of polyphenols in white wines by liquid chromatography: application to the characterization of alella (Catalonia, Spain) wines using chemometric methods, *J. AOAC Int.*, 2017, **100**(2), 323–329, DOI: 10.5740/jaoacint.16-0407.

24 F. de Souza Dias, M. F. Silva and J. M. David, Determination of quercetin, gallic acid, resveratrol, catechin and malvidin in Brazilian wines elaborated in the vale do são francisco using liquid–liquid extraction assisted by ultrasound and GC-MS, *Food Anal. Methods*, 2013, **6**(3), 963–968, DOI: 10.1007/s12161-012-9507-2.

25 M. Piovezan, D. García-Seco, G. A. Micke, J. Gutiérrez-Mañero and B. Ramos-Solano, Method development for determination of (+)-catechin and (−)-epicatechin by micellar electrokinetic chromatography: annual characterization of field grown blackberries, *Electrophoresis*, 2013, **34**(15), 2251–2258, DOI: 10.1002/elps.201300065.

26 R. V. Gottumukkala, N. Nadimpalli, K. Sukala and G. V. Subbaraju, Determination of catechin and epicatechin content in chocolates by high-performance liquid chromatography, *Int. Sch. Res. Notices*, 2014, **2014**, 1–5, DOI: 10.1155/2014/628196.

27 E. Pinilla-Peñalver, M. L. Soriano and A. M. Contento, Á. Ríos. Cyclodextrin-modified graphene quantum dots as a novel additive for the selective separation of bioactive compounds by capillary electrophoresis, *Microchim. Acta*, 2021, **188**(12), 440–462, DOI: 10.1007/s00604-021-05098-0.

28 D. A. Jasim, N. Lozano and K. Kostarelos, Synthesis of few-layered, high-purity graphene oxide sheets from different graphite sources for biology, *2D Mater.*, 2016, **3**(1), 14006–14022, DOI: 10.1088/2053-1583/3/1/014006.

29 A. F. Rodrigues, L. Newman, N. Lozano, S. P. Mukherjee, B. Fadeel, C. Bussy and K. Kostarelos, A blueprint for the synthesis and characterisation of thin graphene oxide with controlled lateral dimensions for biomedicine, *2D Mater.*, 2018, **5**(3), 35020–35038, DOI: 10.1088/2053-1583/aac05c.

30 A. Esteban-Arranz, M. Á. Arranz, M. Morales, R. Martín-Folgar and J. Álvarez-Rodríguez, Thickness of graphene

oxide-based materials as a control parameter, *Chemrxiv*, preprint, 2021, DOI: 10.26434/chemrxiv-2021-sp4zs.

31 M. Dresselhaus, A. Jorio, A. Souza Filho and R. Saito, Defect characterization in graphene and carbon nanotubes using Raman spectroscopy, *Philos. Trans. R. Soc., A*, 2010, **368**(1932), 5355–5377, DOI: 10.1098/rsta.2010.0213.

32 D. López-Díaz, M. López Holgado, J. L. García-Fierro and M. M. Velázquez, Evolution of the Raman spectrum with the chemical composition of graphene oxide, *J. Phys. Chem. C*, 2017, **121**(37), 20489–20497, DOI: 10.1021/acs.jpcc.7b06236.

33 V. Ţucureanu, A. Matei and A. M. Avram, FT-IR spectroscopy for carbon family study, *Crit. Rev. Anal. Chem.*, 2016, **46**(6), 502–520, DOI: 10.1080/10408347.2016.1157013.

34 E. Fuente, J. Menéndez, M. Díez, D. Suárez and M. Montes-Morán, Infrared spectroscopy of carbon materials: a quantum chemical study of model compounds, *J. Phys. Chem. B*, 2003, **107**(26), 6350–6359, DOI: 10.1021/jp027482g.

35 D. W. Chang, E. K. Lee, E. Y. Park, H. Yu, H. J. Choi, I. Y. Jeon, G. J. Sohn, D. Shin, N. Park and J. H. Oh, Nitrogen-doped graphene nanoplatelets from simple solution edge-functionalization for n-type field-effect transistors, *J. Am. Chem. Soc.*, 2013, **135**(24), 8981–8988, DOI: 10.1021/ja402555n.

36 F. F. Liu, J. Zhao, S. Wang, P. Du and B. Xing, Effects of solution chemistry on adsorption of selected pharmaceuticals and personal care products (PPCPs) by graphenes and carbon nanotubes, *Environ. Sci. Technol.*, 2014, **48**(22), 13197–13206, DOI: 10.1021/es5034684.

37 P. V. Kumar, N. M. Bardhan, S. Tongay, J. Wu, A. M. Belcher and J. C. Grossman, Scalable enhancement of graphene oxide properties by thermally driven phase transformation, *Nat. Chem.*, 2014, **6**(2), 151–158, DOI: 10.1038/nchem.1820.

38 S. Srisantitham, M. Sukwattanasinitt and S. Unarunotai, Effect of pH on fluorescence quenching of organic dyes by graphene oxide, *Colloids Surf. A Physicochem. Eng. Asp.*, 2018, **550**, 123–131, DOI: 10.1016/j.colsurfa.2018.04.047.

39 D. K. Ji, Y. Zhang, X. P. He and G. R. Chen, An insight into graphene oxide associated fluorogenic sensing of glycodye–lectin interactions, *J. Mater. Chem. B*, 2015, **3**(32), 6656–6661, DOI: 10.1039/C5TB01162K.

40 P. Drössler, W. Holzer, A. Penzkofer and P. Hegemann, pH dependence of the absorption and emission behaviour of riboflavin in aqueous solution, *Chem. Phys.*, 2002, **282**(3), 429–439, DOI: 10.1016/S0301-0104(02)00731-0.

41 A. M. Hyde, S. L. Zultanski, J. H. Waldman, Y. L. Zhong, M. Shevlin and F. Peng, General principles and strategies for salting-out informed by the Hofmeister series, *Org. Process Res. Dev.*, 2017, **21**(9), 1355–1370, DOI: 10.1021/acs.oprd.7b00197.

42 R. Banerjee, R. Sinha and P. Purkayastha, β-Cyclodextrin encapsulated coumarin 6 on graphene oxide nanosheets: impact on ground-state electron transfer and excited-state energy transfer, *ACS Omega*, 2019, **4**(14), 16153–16158, DOI: 10.1021/acsomega.9b02335.

43 J. L. Chen, X. P. Yan, K. Meng and S. F. Wang, Graphene oxide based photoinduced charge transfer label-free near-infrared fluorescent biosensor for dopamine, *Anal. Chem.*, 2011, **83**(22), 8787–8793, DOI: 10.1021/ac2023537.

44 Y. Liu, C. Y. Liu and Y. Liu, Investigation on fluorescence quenching of dyes by graphite oxide and graphene, *Appl. Surf. Sci.*, 2011, **257**(13), 5513–5518, DOI: 10.1016/j.apsusc.2010.12.136.

45 A. Wesełucha-Birczyńska, K. Morajka, E. Stodolak-Zych, E. Długoń, M. Dużyja, T. Lis, M. Gubernat, M. Ziąbka and M. Błażewicz, Raman studies of the interactions of fibrous carbon nanomaterials with albumin, *Spectrochim. Acta, Part A*, 2018, **196**, 262–267, DOI: 10.1016/j.saa.2018.02.027.

46 M. Paillet, R. Parret, J. L. Sauvajol and P. Colomban, Graphene and related 2D materials: an overview of the Raman studies, *J. Raman Spectrosc.*, 2018, **49**(1), 8–12, DOI: 10.1002/jrs.5295.

47 J. R. Lakowicz, *Principles of Fluorescence Spectroscopy*, Springer Science & Business media, New York, 2nd edn, 2013.

48 L. Wang, R. Liu, Z. Chi, B. Yang, P. Zhang and M. Wang, Spectroscopic investigation on the toxic interactions of Ni^{2+} with bovine hemoglobin, *Spectrochim. Acta, Part A*, 2010, **76**(2), 155–160, DOI: 10.1016/j.saa.2010.03.006.

49 J. Makowska, K. Żamojć, D. Wyrzykowski, D. Uber, M. Wierzbicka, W. Wiczk and L. Chmurzyński, Binding of Cu (II) ions to peptides studied by fluorescence spectroscopy and isothermal titration calorimetry, *Spectrochim. Acta, Part A*, 2016, **153**, 451–456, DOI: 10.1016/j.saa.2015.08.016.

50 I. Lammers, V. Lhiaubet-Vallet, F. Ariese, M. A. Miranda and C. Gooijer, Binding of naproxen enantiomers to human serum albumin studied by fluorescence and room-temperature phosphorescence, *Spectrochim. Acta, Part A*, 2013, **105**, 67–73, DOI: 10.1016/j.saa.2012.12.007.

51 J. Zhang, X. Lu, Y. Lei, X. Hou and P. Wu, Exploring the tunable excitation of QDs to maximize the overlap with the absorber for inner filter effect-based phosphorescence sensing of alkaline phosphatase, *Nanoscale*, 2017, **9**(40), 15606–15611, DOI: 10.1039/C7NR03673F.

52 I. Kaur, V. Batra, N. K. R. Bogireddy, S. Torres and V. Agarwal, Detection of organic pollutants, food additives and antibiotics using sustainable carbon dots, *Food Chem.*, 2023, **406**, 135029–135045, DOI: 10.1016/j.foodchem.2022.135029.

53 A. M. Díez-Pascual, D. García-García, M. P. San Andrés and S. Vera, Determination of riboflavin based on fluorescence quenching by graphene dispersions in polyethylene glycol, *RSC Adv.*, 2016, **6**(24), 19686–19699, DOI: 10.1039/C5RA25547C.

54 J. N. Miller and J. C. Miller, *Statistics and Chemometrics for Analytical Chemistry*, Pearson education, UK, 7th edn, 2018.